

Excellence in Chemistry Research

Announcing our new flagship journal

- Gold Open Access
- Publishing charges waived
- Preprints welcome
- Edited by active scientists



Meet the Editors of *ChemistryEurope*



Luisa De Cola

Università degli Studi
di Milano Statale, Italy



Ive Hermans

University of
Wisconsin-Madison, USA



Ken Tanaka

Tokyo Institute of
Technology, Japan

Switching Chirophilic Self-assembly: From *meso*-structures to Conglomerates in Liquid and Liquid Crystalline Network Phases of Achiral Polycatenar Compounds

Mohamed Alaasar,^{*[a, b]} Yu Cao,^{*[c]} Yan Liu,^[c, d] Feng Liu,^[c] and Carsten Tschierske^{*[a]}

Abstract: Spontaneous generation of chirality from achiral molecules is a contemporary research topic with numerous implications for technological applications and for the understanding of the development of homogeneous chirality in biosystems. Herein, a series of azobenzene based rod-like molecules with an 3,4,5-trialkylated end and a single *n*-alkyl chain involving 5 to 20 aliphatic carbons at the opposite end is reported. Depending on the chain length and temperature these achiral molecules self-assemble into a series of liquid and liquid crystalline (LC) helical network phases. A chiral isotropic liquid (Iso₁^[*]) and a cubic triple network phase with chiral *I*23 lattice were found for the short chain compounds, whereas non-cubic and achiral cubic phases dominate for the long chain compounds. Among them a mesoscale conglomerate

with *I*23 lattice, a tetragonal phase (Tet_b) containing one chirality synchronized and one non-synchronized achiral network, an achiral double network *meso*-structure with *la* $\bar{3}$ *d* space group and an achiral percolated isotropic liquid mesophase (Iso₁) were found. This sequence is attributed to an increasing strength of chirality synchronization between the networks, combined with a change of the preferred mode of chirophilic self-assembly between the networks, switching from enantiophilic to enantiophobic with decreasing chain length and lowering temperature. These nanostructured and mirror symmetry broken LC phases exist over wide temperature ranges which is of interest for potential applications in chiral and photosensitive functional materials derived from achiral compounds.

Introduction

Functional materials based on helical assemblies are required for photonic band-gap materials, for materials with chiroptical properties, capability of chiral recognition and chiral emission.^[1,2] These applications require chiral compound, which

are expensive to synthesize and often only available in one of the enantiomeric forms. However, in the process of mirror symmetry breaking, chirality develops spontaneously from achiral or racemic sources, and the sense of chirality can be tuned and fixed by application of chiral dopants or chiral physical forces by means of asymmetry amplification. This was first recognized in crystalline solid-state assemblies^[3,4] and more recently expanded to aggregation of crystalline fibres in dilute solution^[4,5] and gels in solvent-swollen systems.^[6] Liquid crystals, (LCs)^[7,8] on the other hand, are soft functional materials that combine molecular order and mobility, making them relevant for numerous applications in functional devices, among them, displays, light modulating and sensor devices.^[9] The reduced order and increased mobility of the molecules in the LC state would be expected to reduce their chiral recognition capability in these systems. Nevertheless, spontaneous generation of macroscopic homochirality was in the recent decade discovered in LCs^[10] of bent-core molecules,^[11–14] dimesogens^[15,16] and specifically designed polycatenar molecules.^[17] For the latter mirror symmetry breaking was even found in the isotropic liquids state,^[18–20] which is of relevance for the understanding of the emergence of biochirality.^[20,21]

In these polycatenar compounds, a rod-like π -conjugated polyaromatic core-structure is decorated with a number of 3 to 6 alkyl chains distributed to both ends.^[22] The rod-like moieties of these molecules can align side by side, thus forming columnar aggregates,^[10,17] in which the rod-like cores are arranged predominately perpendicular to the column long axis. The clashing of the bulky aliphatic end-chains leads to a twist between adjacent rafts of molecules, giving rise to a helical

[a] Prof. Dr. M. Alaasar, Prof. Dr. C. Tschierske
Institute of Chemistry
Martin-Luther University Halle-Wittenberg
Kurt-Mothes Str. 2, D-06120 Halle/Saale (Germany)
E-mail: carsten.tschierske@chemie.uni.halle.de

[b] Prof. Dr. M. Alaasar
Department of Chemistry
Faculty of Science
Cairo University
P.O. 12613 Giza (Egypt)
E-mail: malaasar@sci.cu.edu.eg

[c] Dr. Y. Cao, Y. Liu, Prof. Dr. F. Liu
Shaanxi International Research Center for Soft Matter
State Key Laboratory for Mechanical Behavior of Materials
Xi'an Jiaotong University
Xi An Shi, Xi'an 710049 (P. R. China)
E-mail: yu.cao@xjtu.edu.cn

[d] Y. Liu
Wanhua Chemical Group Co
Ltd., Yantai 265505 (P. R. China)

Supporting information for this article is available on the WWW under <https://doi.org/10.1002/chem.202201857>

© 2022 The Authors. Chemistry - A European Journal published by Wiley-VCH GmbH. This is an open access article under the terms of the Creative Commons Attribution Non-Commercial License, which permits use, distribution and reproduction in any medium, provided the original work is properly cited and is not used for commercial purposes.

superstructure along the columns, which is supported by the chirality synchronization of the helical conformers of the involved molecules.^[10,23,24] However, in columnar phases there are numerous helix sign inversions which cancel long-range helicity, and hence the columnar LC phases are usually achiral on a macroscopic scale.^[10,25] Only in few cases at low temperature through-space coupling between the columns can lead to long range helicity,^[26,27] in most cases after transition to a soft crystalline mesophase.^[28,29]

In contrast, the bicontinuous cubic (Cub_{bi}) LC phases represent networks of branched columns (Figure 1).^[30-35] In the Cub_{bi} phases of polycatenar molecules the junctions of the networks transmit chirality by removing helix-reversal defects and thus lead to long range helicity and uniform chirality along the networks.^[10,17,36] Presently there are two known Cub_{bi} phases of polycatenar molecules. The $Ia\bar{3}d$ phase (double gyroid) is composed of two enantiomorphous helical networks and there-

fore represents an achiral *meso*-structure (Figure 1a), i.e. there is enantiophilic coupling between the networks (heterochiral self-assembly).^[17,36] In contrast, the $I23$ phase^[37-42] being composed of three networks (Figure 1b) is chiral and typically forms a conglomerate of chiral domains ($Cub_{bi}/I23^{*k}$), meaning that the network coupling becomes enantiophobic (homochiral self-assembly) and mirror symmetry is broken by the formation of a conglomerate of chiral domains.^[10,17,19,43-49] Most compounds forming these mirror symmetry broken LC phases represent derivatives of 5,5'-diphenyl-2,2'-bithiophene^[17,18,38,39,50] or 1,2-diphenylethane-1,2-dione (benzil).^[51,52] More recently hydrogen bonded supramolecules^[53] and compounds involving functional units, such as charge carriers (BTBT)^[54] or photosensitive and photoisomerizable azobenzene units were also introduced.^[55-57] For one of these polycatenar azobenzenes **A10/18** (see Scheme 1, $n=18$) a new tetragonal LC phase was discovered.^[58] Its structure was proven to represent a non-cubic bicontinuous double network structure (Tet_{bi}) composed of a pair of chiral $P4_212$ and $P4_32_12$ space groups. In this case one network is chiral whereas the other one is racemized and this structure is considered as an intermediate step of the transition between enantiophilic and enantiophobic self-assembly.

Herein we provide an understanding of the effects of the molecular structure on the spontaneous emergence of chirality and the transition between the two different modes of chirophilic interhelical self-assembly, being either enantiophilic or enantiophobic, which is of importance for the design of spontaneously mirror symmetry broken functional materials. To this end the series of taper shaped azobenzene-based polycatenars **A10/ n** (Scheme 1) with a length of the terminal single chain n ranging from $n=5$ to $n=20$ was synthesized and investigated.

Results

Synthesis and materials

The synthesis of the azobenzene-based polycatenars **A10/ n** (Scheme 1) was performed in an analogous way to that reported previously^[36,56] from 4'-hydroxybiphenyl-4-yl 3,4,5-tri-*n*-decyloxybenzoate (**2**)^[59] and the 4-(4-alkoxyphenyldiazanyl)benzoic acids **1/ n** ($n=5-12$, 18,^[60] $n=14,16$ ^[61,62]). Compounds **1/ n** were synthesized by Williamson etherification of ethyl 4-(4-hydroxyphenyldiazanyl)benzoate^[63] with 1-bromo-*n*-alkanes, followed by hydrolysis.^[61,62] Due to low solubility of these benzoic acids **1/ n** in most organic solvents, neat $SOCl_2$ was used as activating agent for the acylation reaction with the phenol **2** as described in the Experimental Section.

The compounds **A10/ n** were investigated by polarizing optical microscopy (POM), differential scanning calorimetry (DSC) and X-ray diffraction (XRD) as described in the Experimental Section. The phase sequences and transition temperatures of compounds **A10/ n** are collected in Table 1 and shown graphically in Figure 2. The compounds can be divided into two groups, the short-chain compounds with $n=5-12$ and the long

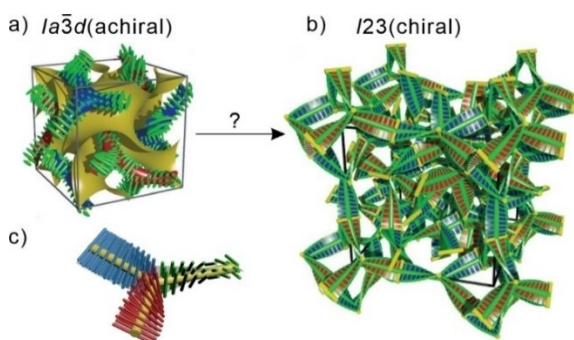
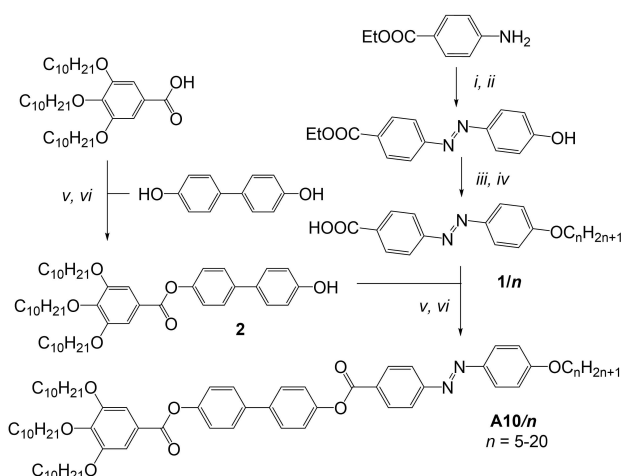
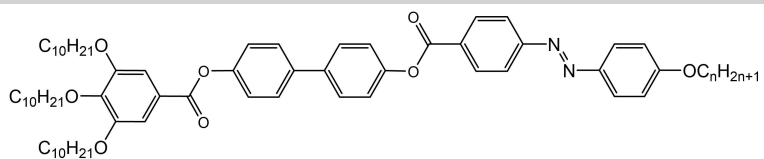


Figure 1. Helical network structures of the Cub_{bi} phases under discussion a) *meso*-structure with $Ia\bar{3}d$ space group (double gyroid) and b) chiral $I23^{*k}$ phase^[37] forming a conglomerate.^[17] Both network structures are composed of three-way junctions; c) a schematic representation of a three-way junction interconnecting three network segments formed by the helical stacking of rafts of three molecules.



Scheme 1. Synthesis of compounds **A10/ n** . Reagents and conditions: i: $NaNO_2$, HCl , H_2O , $0 \rightarrow 5^\circ C$, 30 min; ii: 1. phenol, $NaOH$, $5 \rightarrow 20^\circ C$, 1 h, 2. $NaHCO_3$; iii: $C_nH_{2n+1}Br$, KI , K_2CO_3 , 2-butanone, reflux, 18 h; iv: $EtOH$, KOH , reflux, 8 h; v: $SOCl_2$, DMF , reflux 1 h.; vi: dry CH_2Cl_2 , dry TEA , dry pyridine, reflux, 6 h.

Table 1. Phase transition temperatures ($T/^\circ\text{C}$), mesophase types, and transition enthalpies [$\Delta H/\text{kJ mol}^{-1}$] of compounds **A10/n**.


Compd.	n	Phase sequence
A10/5	5	Cr 78 [45.0] $\text{Cub}_{\text{bi}}/I23^{[*]}$ 168 [1.2] $\text{Iso}_1^{[*]}$ 171 [0.4] Iso Iso 169 [−0.7] $\text{Iso}_1^{[*]}$ 156 [−0.7] $\text{Cub}_{\text{bi}}/I23^{[*]}$ < 20 Cr
A10/6	6	Cr 88 [94.1] $\text{Cub}_{\text{bi}}/I23^{[*]}$ 167 [1.7] Iso Iso 167 [−0.5] $\text{Iso}_1^{[*]}$ 156 [−1.0] $\text{Cub}_{\text{bi}}/I23^{[*]}$ < 20 Cr
A10/7	7	Cr 87 [22.2] $\text{Cub}_{\text{bi}}/I23^{[*]}$ 166 [2.0] Iso Iso 164 [−0.5] $\text{Iso}_1^{[*]}$ 156 [−0.9] $\text{Cub}_{\text{bi}}/I23^{[*]}$ 23 [−22.7] Cr
A10/8	8	Cr 99 [39.8] $\text{Cub}_{\text{bi}}/I23^{[*]}$ 165 [1.4] Iso Iso 163 [−0.5] $\text{Iso}_1^{[*]}$ 156 [−0.7] $\text{Cub}_{\text{bi}}/I23^{[*]}$ 16 [−11.2] Cr
A10/9	9	Cr 86 [37.8] $\text{Cub}_{\text{bi}}/I23^{[*]}$ 163 [1.8] Iso Iso 159 [−0.5] $\text{Iso}_1^{[*]}$ 153 [−1.0] $\text{Cub}_{\text{bi}}/I23^{[*]}$ 21 [−8.1] Cr
A10/10	10	Cr 76 [49.3] $\text{Cub}_{\text{bi}}/I23^{[*]}$ 163 [2.0] Iso Iso 160 [−0.5] $\text{Iso}_1^{[*]}$ 156 [−1.2] $\text{Cub}_{\text{bi}}/I23^{[*]}$ 20 [−3.8] Cr
A10/12	12	Cr 72 [50.7] $\text{Cub}_{\text{bi}}/I23^{[*]}$ 165 [2.2] $\text{Iso}_1 \sim 175$ [1.9] Iso Iso 170 [−2.2] Iso_1 162 [−0.7] $\text{Iso}_1^{[*]}$ 156 [−1.1] $\text{Cub}_{\text{bi}}/I23^{[*]}$ 22 [−6.7] Cr
A10/14	14	Cr 51 [29.6] X 77 [−] $\text{Cub}_{\text{bi}}/I23 \sim 127$ [−] $\text{Tet}_{\text{bi}} \sim 147$ [−] $\text{Cub}/Ia\bar{3}d$ 157 [2.5] $\text{Iso}_1 \sim 170$ [2.5] Iso Iso ~ 165 [−2.4] Iso_1 149 [−0.5] $\text{Iso}_1^{[*]}$ 144 [−1.0] $\text{Cub}/Ia\bar{3}d \sim 140$ [−] Tet_{bi} 30 [−8.6] Cr
A10/16	16	Cr 67 [49.0] X ~ 75 [−] $\text{Cub}_{\text{bi}}/I23 \sim 107$ [−] $\text{Tet}_{\text{bi}} \sim 112$ [−] $\text{Cub}_{\text{bi}}/Ia\bar{3}d$ 157 [2.9] $\text{Iso}_1 \sim 170$ [2.9] Iso Iso ~ 167 [−3.6] Iso_1 147 Col 144 [−1.8] ^b $\text{Cub}_{\text{bi}}/Ia\bar{3}d$ 105 [−] Tet_{bi} 28 [−19.9] Cr
A10/18 ^[36,58]	18	Cr 64 [51.2] X78 [−] $\text{Cub}_{\text{bi}}/I23 \sim 95$ [−] $\text{Tet}_{\text{bi}} \sim 135$ [−] $\text{Cub}_{\text{bi}}/Ia\bar{3}d \sim 157$ [2.8] $\text{Iso}_1 \sim 169$ [3.2] Iso Iso ~ 165 [−3.5] Iso_1 150 [−1.6] Col_{hex} 145 [−0.4] $\text{Cub}_{\text{bi}}/Ia\bar{3}d \sim 135$ [−] Tet_{bi} 36 [−25.5] Cr
A10/20	20	Cr 71 [55.0] $\text{Cub}_{\text{bi}}/Ia\bar{3}d$ 156 [2.8] $\text{Iso}_1 \sim 167$ [2.3] Iso Iso ~ 165 [−4.2] Iso_1 152 [−1.9] Col_{hex} 144 [−0.3] $\text{Cub}_{\text{bi}}/Ia\bar{3}d \sim 135$ [−] Tet_{bi} 43 [−28.8] Cr

^a Peak temperatures as determined from 2nd heating (upper lines) and 2nd cooling (lower lines) DSC scans with rate 10 K min^{−1}; all transitions without visible ΔH were taken from continuous XRD scans in combination with optical investigations, these are approximate values, because there is a strong dependence on conditions and sample history; for the broad Iso–Iso₁ transitions the middle of the broad DSC feature is given. Abbreviations: Cr = crystalline solid (most compounds show only partial crystallization on cooling); X = unknown phase; Iso = achiral isotropic liquid; Iso₁ = achiral percolated isotropic liquid phase; Iso₁^[*] = ambidextrous chiral isotropic liquid phase; $\text{Cub}_{\text{bi}}/Ia\bar{3}d$ = achiral bicontinuous cubic phase with $Ia\bar{3}d$ space group (double gyroid); $\text{Cub}_{\text{bi}}/I23^{[*]}$ = ambidextrous chiral bicontinuous cubic phase with $I23$ space group; $\text{Cub}_{\text{bi}}/I23$ = macroscopically achiral $\text{Cub}_{\text{bi}}/I23$ phase; Tet_{bi} = tetragonal phase representing a pair of chiral space groups $P4_12_1/P4_32_1$; Col_{hex} = hexagonal columnar phase. Enthalpy value involves both transitions, Iso₁– Col_{hex} and Col_{hex} – Cub_{bi} .

chain compounds with $n = 14$ – 20 , which are described separately in the two following sections.

Short chain compounds A10/5–A10/12

Chiral liquid crystalline cubic phase. – In the DSC heating traces of compounds **A10/5**–**A10/12** (see Figure 3a,b for examples) only one sharp transition around 162–168 °C with an enthalpy of 1.4–2.2 kJ mol^{−1} is observed besides the melting event. The transition enthalpy increases with growing n , while the transition temperatures are almost constant and only slightly decrease without any noticeable odd-even effect (Table 1). At this transition the viscosity of the optically isotropic sample suddenly decreases as typical for a transition of a cubic mesophase at lower temperature to the isotropic liquid at higher.

The small angle X-ray scattering pattern (SAXS) of this cubic phase is indexed in all cases with $n = 5$ – 12 to the $I23$ space group^[37] with a lattice parameter a_{cub} between 17.8 and 18.4 nm (Table 2). Figure 4a shows the indexed SAXS pattern of compound **A10/6** as an example. The SAXS data of the other homologues with $n = 8$ – 12 are collated in Figures S8–S10 and

Tables S2–S4 in the Supporting Information. Electron density (ED) reconstruction of the SAXS pattern indicates a bicontinuous cubic phase (Cub_{bi}) with triple network structure and three-way junctions (Figure 4b,c). In the wide-angle range (WAXS) there is only one diffuse scattering with a maximum around $d = 0.45$ nm for all compounds (Figure S11), confirming the absence of fixed positions for individual molecules and thus the liquid crystalline state of this cubic phase. For all $\text{Cub}_{\text{bi}}/I23^{[*]}$ phases of compounds **A10/5**–**A10/12** a conglomerate of chiral domains can be observed by polarizing optical microscopy (Figure 5c,d). Accordingly, after rotating the analyser by a small angle (1–5°) out of the 90° crossed orientation the formation of dark and bright domains is observed, which invert their brightness upon rotating the polarizer with the same angle into the opposite direction. This confirms the ambidextrous mirror symmetry breaking in this cubic phase ($\text{Cub}_{\text{bi}}/I23^{[*]}$).

This mirror symmetry broken Cub_{bi} phase is stable over a broad temperature range and no other LC phase is observed. For compounds **A10/10** and **A10/12** the crystallization is very slow and their Cub_{bi} phases can be observed down to ambient temperature (25 °C), even after storing the samples for several months at this temperature no crystallization is observed

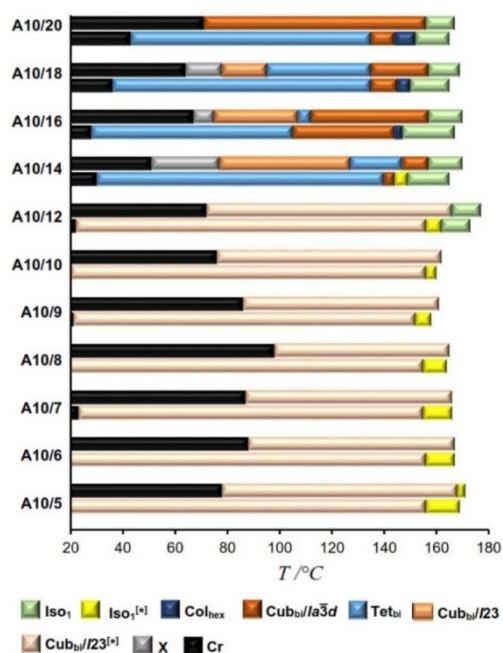


Figure 2. Bar diagram showing the mesophases and phase transition temperatures of series A10/*n* on heating (upper bars) and on cooling (lower bars); for abbreviations see Table 1; the ordinary isotropic liquid (Iso) is in all cases at the right side of the bars.

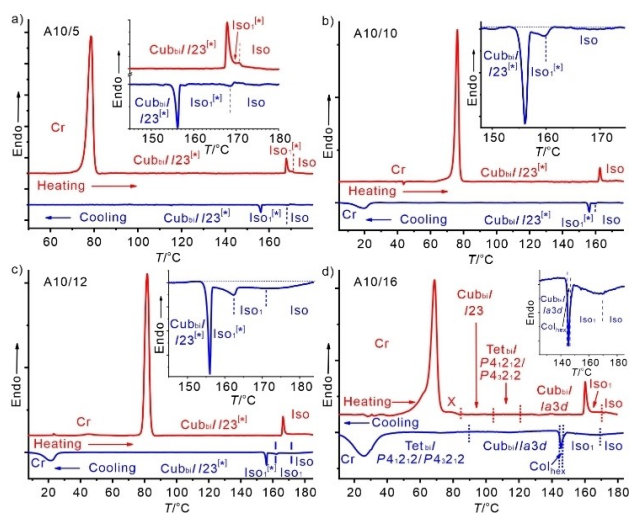


Figure 3. DSC second heating and cooling traces at a rate of 10 K min⁻¹ for selected compounds showing different types of Iso-Cub_{bi} transitions: a) A10/5 and b) A10/10 short chain compounds with Iso-Iso₁^[*] liquid state diamorphism, c) A10/12 with liquid state triamorphism and d) long chain compound A10/16 with Iso-Iso₁-(Col_{hex})-Cub_{bi} transition. In the cooling scan of A10/16 the Cub_{bi}-Col_{hex} and Col_{hex}-Iso₁ transitions cannot be separated.

(Figure 2 and Table 1). This makes these materials excellent candidates for potential technological applications

Polyamorphism and mirror symmetry breaking in the liquid state. – Compounds A10/6–A10/10 show a direct transition from the Cub_{bi}/I23^[*] phase to the isotropic liquid state (Iso) on heating, whereas on cooling a small range of a

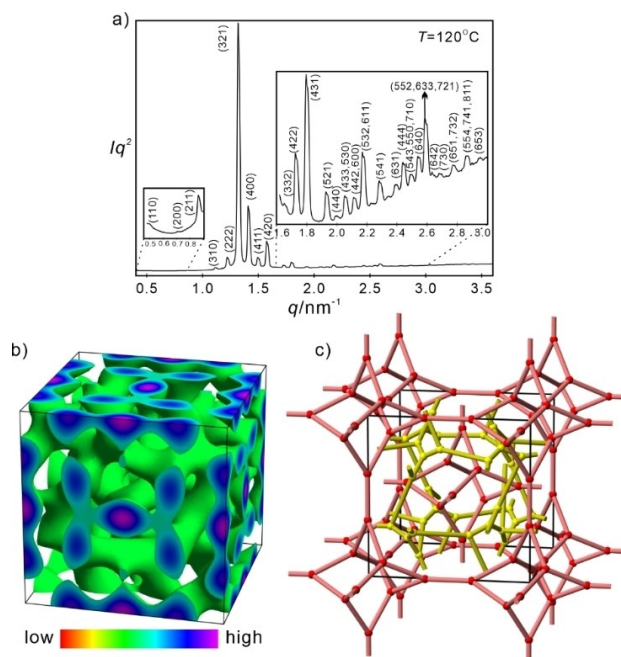


Figure 4. a) SAXS diffractogram of A10/6 on heating at $T = 120\text{ }^{\circ}\text{C}$ in the Cub_{bi}/I23^[*] phase, b) the reconstructed 3D electron density map and c) schematic presentation of the triple network structure. The inner and outer networks in red are same with each other and the middle network in yellow lies on the Schwarz P minimal surface; thus, the interpenetrated networks in red provide a structure related to the Plumber's Nightmare cubic lattice^[30] with complex polyhedral frameworks – involving exclusively three way junctions – forming the nodes.

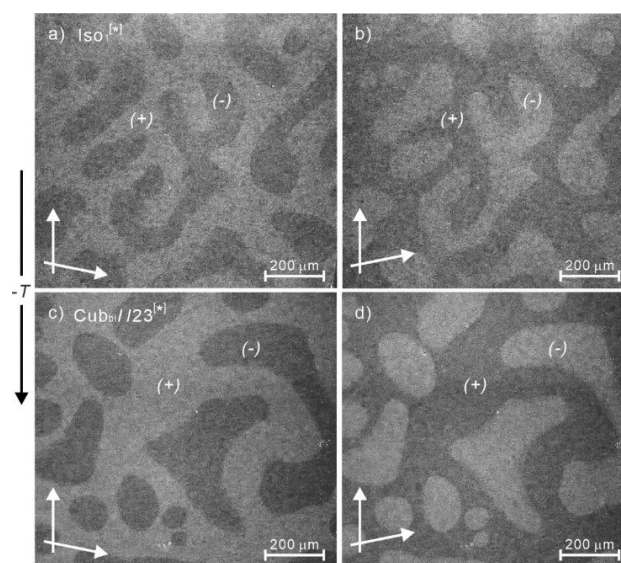


Figure 5. Textures of A10/12 as observed by polarizing microscopy between two microscopy glass slides (sample thickness about 50 μm) upon cooling from Iso, a, b) in the Iso₁^[*] phase at 162 °C and c, d) in the Cub_{bi}/I23^[*] phase as formed from Iso₁^[*] at 145 °C; a, c) after rotating one of the analysers by 5° in clockwise direction and b, d) after rotating one of the analysers by 5° in anticlockwise direction out of the 90° crossed positions; the arrows indicate the directions of polarizer and analyzer; a, b) and c, d) show the same area, but due to the mobility of the domain boundaries in the Iso₁^[*] temperature range they move and change their shape, and therefore a, b) and c, d) appear different; all photos were transformed to grey scale and the contrast was enhanced.

Table 2. Selected structural data of the mesophases of the investigated compounds, for a complete list and detailed calculations, see Table S11).^a

Comp.	Temp. [°C]	Phase	a/nm	n_{raft}	$\Phi/^\circ$
A10/6	120	$I23$	17.78	3.6	7.85
A10/8	140	$I23$	17.68	3.5	7.89
A10/10	100	$I23$	18.26	3.6	7.65
A10/12	100	$I23$	18.44	3.6	7.57
A10/14	157	$la\bar{3}d$	11.14	3.2	8.06
	140	Tet_{bi}	$a = 11.18$ $c = 12.07$	3.4	7.75
A10/16	110	$I23$	18.19	3.5	7.68
	125 (cooling)	$la\bar{3}d$	11.14	3.2	8.06
	95 (heating)	$I23$	17.96	3.4	7.78
	90 (cooling)	Tet_{bi}	$a = 11.19$ $c = 12.08$	3.4	7.74
A10/18	150	$la\bar{3}d$	11.23	3.3	7.99
	130	Tet_{bi}	$a = 11.21$ $c = 11.72$	3.4	7.85
A10/20	85	$I23$	18.66	3.7	7.48
	125	$la\bar{3}d$	11.45	3.3	7.83

^a For XRD data, see Tables S1–S10 and Figures S7–S13.

mirror symmetry broken isotropic liquid ($Iso_1^{[*]}$) is observed (Figures 2 and 5a, b and Table 1). Similar to the $Cub_{bi}/I23^{[*]}$ phase it is indicated by a conglomerate of chiral domains with the difference that these domains easily flow, while they do not in the cubic phase. The $Cub_{bi}/I23^{[*]}$ phase develops from this liquid conglomerate phase with smoothly curved boundaries (Figure 5c, d). In contrast, if the $Cub_{bi}/I23^{[*]}$ phase would be directly formed from the achiral isotropic liquid, then straight phase boundaries between the chiral domains would evolve (see ref. [17] for examples). As shown in the DSC traces of compounds A10/5 and A10/10 (Figure 3a, b), the typical feature of the $Iso-Iso_1^{[*]}$ transition, associated with the onset of mirror symmetry breaking, is a relatively small peak (the “bump”) followed by a long tailing over almost 10 K (total ΔH is around 0.5 kJ mol^{-1}). The bump at the beginning of the broad DSC feature is associated with the onset of chirality synchronization, leading to mirror symmetry breaking and conglomerate formation at this transition. The tailing is attributed to the further growing network connectivity until at a certain critical network density the cubic 3D lattice is formed at the next sharp transition ($\Delta H = 0.7\text{--}1.2 \text{ kJ mol}^{-1}$) on further cooling (Figure 6). This means that ambidextrous mirror symmetry breaking sets in already in the temperature range of the isotropic liquid state

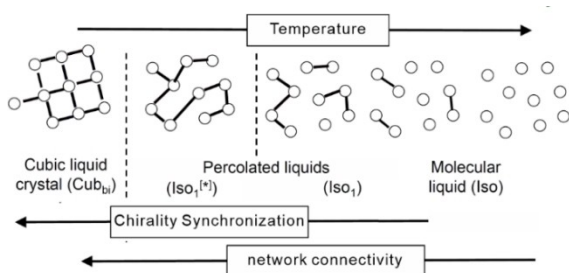


Figure 6. Development of network connectivity during the transition from Iso via Iso_1 and $Iso_1^{[*]}$ to Cub_{bi} .^[51]

before the long-range cubic lattice with $I23$ space group is formed. Only for compound A10/5 a small range of the $Iso_1^{[*]}$ phase of about 2 K can also be observed on heating (see inset in Figure 3a) as an enantiotropic $Iso_1^{[*]}$ phase range. For all other compounds it is a monotropic phase, only found on cooling, i.e. it is metastable with respect to the $Cub_{bi}/I23^{[*]}$ phase. The monotropic $Iso_1^{[*]}$ range becomes smaller with growing chain length n (from 13 to 5 K, see Figure 2). It is accompanied by an achiral Iso_1 phase for $n = 12$ and 14, and it vanishes for $n = 16$ and the following homologues.

Long chain compounds A10/14–A10/20

Liquid crystalline polymorphism (mesophases with 3D lattice). – For compound A10/14 and the following homologues with $n = 16\text{--}20$ different phase sequences were observed which are much more complicated than those of the short chain compounds (Table 1 and Figure 2). For these compounds there are several transitions between different mesophases with 3D lattice which are slow and therefore not visible in the DSC traces. Moreover, many of these transitions are strongly dependent on the conditions (sample history, sample thickness, heating and cooling rates, etc.), some phases are metastable and different coexisting structures are involved. Therefore, for these transitions without visible enthalpy change in the DSC traces only approximate transition temperatures can be provided. For A10/16 as an example (Figure 3d), after melting of the crystals at 67°C the birefringence decreases in the temperature range indicated as “X range” and the sample becomes optically isotropic at the transition to the $Cub_{bi}/I23$ phase at 75°C . A weak birefringence re-appears at the next transition at 107°C to Tet_{bi} and at 112°C the compound becomes optically isotropic again at the transition to the $Cub_{bi}/la\bar{3}d$ phase. Only the transition to the isotropic liquid state is associated with a sharp DSC peak at 157°C and $\Delta H = 2.9 \text{ kJ mol}^{-1}$. There is an additional broad feature in the isotropic

liquid range around 170 °C which is attributed to a liquid state polymorphism due to the continuous disintegration of the network structure into ever smaller domains (Figure 6). On cooling this broad feature is also observed and followed by a sharp peak at 144–147 °C ($\Delta H = 1.8 \text{ kJ mol}^{-1}$), involving the transition to a birefringent Col_{hex} phase (Figure 7a) which is immediately replaced by the quickly growing $\text{Cub}_{\text{bi}}/la\bar{3}d$ phase (Figures 7b and S6d). Upon further cooling, birefringence sets in at 105 °C corresponding to the $\text{Cub}_{\text{bi}}/la\bar{3}d$ to Tet_{bi} phase transition (Figure 7c) and partial crystallization starts around 30 °C. For all compounds **A10/14–A10/18** the $\text{Cub}_{\text{bi}}/I23$ phase is only formed upon heating the birefringent crystalline solid and passing an unknown “X range” (see Figure 2). In this X-range there is a broad SAXS scattering, combined with sharp reflections (Figures S12a–S13a). In line with optical investigations it is interpreted as a temperature range where the birefringent crystalline phase coexists with an optically isotropic disordered structure. Upon increasing temperature, the diffuse SAXS as well as the sharp peaks in the X range are slowly replaced by the typical sharp scattering peaks of the *I23* phase. The temperature at which all scatterings associated with the X-range have disappeared and the sample has become completely isotropic is denoted as the X to *I23* transition temperature.

The lattice parameter of the *I23* phase of **A10/14–A10/18** is $a_{\text{cub}} = 18.0\text{--}18.7 \text{ nm}$ which is in the same range as observed for the shorter homologues (Table 2). The SAXS patterns of the *I23* phase of these long chain compounds (Figures S12b–S13b) are identical with each other and with those recorded for the related compounds with shorter chains. However, no chiral domain can be observed for any of the *I23* phases of compounds **A10/14–A10/18**, even if very thick samples ($\sim 100 \mu\text{m}$) were investigated. This is the first case where no macroscopic conglomerate formation can be found in the *I23* phase of a polycatenar compound ($\text{Cub}_{\text{bi}}/I23$ phase). Therefore, absence/presence of visible chiral domains cannot be considered as sufficient to classify a Cub_{bi} phase of polycatenar compounds unambiguously to either the $la\bar{3}d$ or *I23* space group; in addition, it needs to be confirmed by SAXS investigation. It is assumed that this cubic phase with chiral *I23* space group still represents a conglomerate, but the size of the chiral domains (according to SAXS the correlation length is 500–1000 nm) is in this case too small to be recognizable by optical investigations in the visible light range. Therefore, this

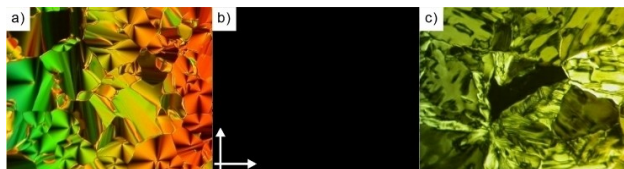


Figure 7. Textures observed under POM as recorded between two microscopy glass plates (distance ca. 10 μm) on cooling for **A10/16** in: a) Col_{hex} phase at 147 °C; b) $\text{Cub}_{\text{bi}}/la\bar{3}d$ phase at 145 °C; c) Tet_{bi} phase at 45 °C; in the dark area the *c*-axis is perpendicular to the substrate. The arrows indicate the directions of polarizer and analyzer, which is identical in all three photos; for additional textures of other compounds, see Figures S5 and S6.

mesoscale conglomerate appears optically inactive on a macroscopic length scale.

Upon heating the isotropic $\text{Cub}_{\text{bi}}/I23$ phase of compounds **A10/14–A10/18** it is replaced by the birefringent tetragonal phase (Tet_{bi}), followed by a cubic $\text{Cub}_{\text{bi}}/la\bar{3}d$ phase. The diffraction pattern of the Tet_{bi} phase is identical for all compounds (see Figure 8a for an example) and this phase has been analysed in detail in our previous report for the case of compound **A10/18**.^[58] Accordingly, this tetragonal phase is derived from the $la\bar{3}d$ double gyroid phase by continuous stretching the lattice along the *c*-direction as shown for **A10/16** in Figure 8b,c. The space group is $P4_12_1/P4_32_12$, which represents a pair of enantiomeric chiral space groups as confirmed by high resolution SAXS, simulated diffraction patterns and by resonant soft X-ray scattering (RSoXS) at the Carbon K-edge.^[58] In all three investigated Tet_{bi} phases the parameter a_{tet} is 11.1–12.5 nm, thus corresponding to a_{cub} of the adjacent $la\bar{3}d$ phase ($a_{\text{cub}} = 11.1\text{--}11.5 \text{ nm}$, Table 2) and the parameter c_{tet} rises with lowering temperature until it reaches 14.3–14.6 nm close to the $\text{Tet}_{\text{bi}}\text{--Cub}_{\text{bi}}/I23$ transition temperature. At the continuous transition to the high temperature cubic phase with $la\bar{3}d$ lattice, the *c*-parameter of the Tet_{bi} phase decreases and becomes identical with a_{tet} (Figures 9a,b, S14). At this temperature the compound becomes optically isotropic, remains highly viscous and no chiral domains can be observed. This indicates the transition to an achiral cubic $la\bar{3}d$ phase, which remains till the final transition to the isotropic liquid takes place at $\sim 157 \text{ °C}$ for all three compounds **A10/14–A10/18**. The SAXS pattern of this high temperature cubic mesophase (Figure 8d) confirms an $la\bar{3}d$ space group with $a_{\text{cub}} = 11.1\text{--}11.5 \text{ nm}$, slightly growing with chain length (Table 2). In the *I23* phase the parameter a_{cub} is 17.7–18.7 nm, corresponding to an increase by 50% compared to a_{cub} in the $\text{Cub}_{\text{bi}}/la\bar{3}d$ phase, in line with the elongation of the networks from a double to a

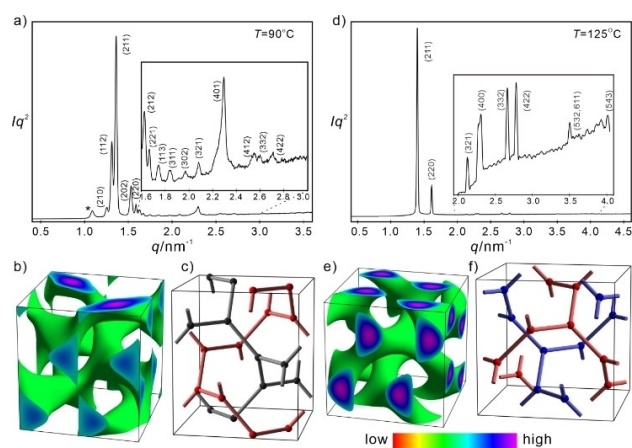


Figure 8. SAXS diffractogram of **A10/16** on cooling: a) in the Tet_{bi} phase at $T = 90 \text{ °C}$ and d) in the $\text{Cub}_{\text{bi}}/la\bar{3}d$ phase at $T = 125 \text{ °C}$ and the corresponding ED maps of the double network phases b) the Tet_{bi} phase and e) the $\text{Cub}_{\text{bi}}/la\bar{3}d$ phase (the asterisk signal in a) is from Cr). Corresponding schematic presentation of their double network structures are provided in c) and f); in f) there are two enantiomeric networks with opposite helicity (blue/red), whereas in e) one of the networks (grey) has a reduced coherence length of helix sense.

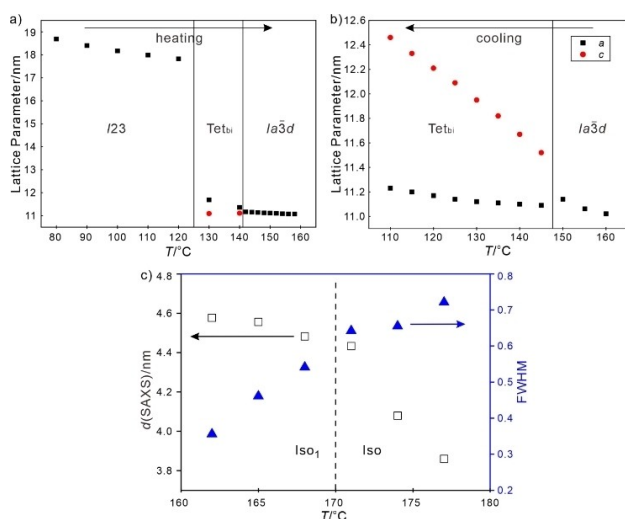


Figure 9. Temperature scans of the SAXS of A10/14. a) Lattice parameter variation of A10/14 and during the phase transition on heating and b) between Tet_{bi} phase and Cub_{bi}/Ia $\bar{3}d$ phase upon cooling; c) shows *d*-spacing and line width at half maximum (FWHM) for the main SAXS reflection as observed on continuous heating in the isotropic liquid state around the Iso₁-Iso transition, see Figure S14 for additional temperature scans.

triple network structure (Figure 1, Table 2). For A10/14 the temperature range of the Ia $\bar{3}d$ cubic phase is only short, but it expands with growing chain length *n*. In contrast, the Cub_{bi}/I23 phase range narrows with growing *n* and has disappeared for *n*=20. This apparently “achiral” I23 phase is metastable with respect to the Tet_{bi} phase and is replaced in its whole temperature range by the birefringent Tet_{bi} phase after about 20–60 minutes storage. The actual time required for this transition decreases with rising temperature. For this reason, the Cub_{bi}/I23 phase is only observed on heating from the crystalline solid in a limited temperature range, while on cooling from the isotropic liquid the Cub_{bi}/Ia $\bar{3}d$ and Tet_{bi} phases were found exclusively (Figure 2). Moreover, the transition Cub_{bi}/I23→Tet_{bi} becomes faster with growing chain length from *n*=14 to *n*=18 and it totally disappears for the longest compound A10/20. For this compound, exclusively a broad region of the Cub_{bi}/Ia $\bar{3}d$ phase is observed on heating. Upon cooling, the Cub_{bi}/Ia $\bar{3}d$ phase, developing from the metastable Col_{hex} phase (see Figure S6c,d), is replaced at 135°C by the birefringent Tet_{bi} phase (Figure S6e) in a similar way as observed for A10/18.

Overall there is a sequence Cub_{bi}/I23^[*]→Cub_{bi}/Ia $\bar{3}d$ +Tet_{bi} upon alkyl chain elongation. The phase sequence Ia $\bar{3}d$ →I23^[*]→Ia $\bar{3}d$ was previously found with growing alkyl chain volume in some other homologous series of rod-like molecules with Cub_{bi} phases.^[32,38–40,44,50,51,64,65] This sequence is usually associated with a continuous increase of the twist angle Φ between the molecules in the rafts forming the helical networks, leading to a phase sequence involving a long pitch (small twist) Ia $\bar{3}d$ (L) phase followed by I23^[*] and a short pitch (large twist) Ia $\bar{3}d$ (S) phase.^[50,51] The same is found in the present case where the twist angle Φ increases from 7.5–7.9° in the I23^[*]/I23 phases to 7.8–8.1° in the Ia $\bar{3}d$ phase (see Table 2),^[66] in line with a short

pitch Ia $\bar{3}d$ (S) type of this phase. This is supported by the observation of an induced I23^[*] phase in the contact region with a long pitch Ia $\bar{3}d$ (L) phase material and its absence in contact with a short pitch Ia $\bar{3}d$ (S) compound (see Figure S15). Thus, increasing chain volume increases the intermolecular twist Φ along the aggregates and this leads to the transition Cub_{bi}/I23^[*]→Cub_{bi}/Ia $\bar{3}d$ upon chain elongation. An increase of Φ is also observed with rising temperature, indicated by a decreasing lattice parameter within the distinct phase ranges as well as jumps at the transitions between the different network phases (see compounds A10/14 and A10/18 in Table 2 and Figure 9a). Thus, the twist Φ increases from I23 via Tet_{bi} to Ia $\bar{3}d$ (S), in line with thermal chain expansion.

Col_{hex} phase. – In addition, for the three longest homologues A10/16–A10/20 a short range of a Col_{hex} phase of ~5–6 K is observed on cooling from the isotropic liquid as a metastable phase before the transition to Cub_{bi}/Ia $\bar{3}d$ phase (Figure 7a). This indicates an increasing intermaterials (aromatics vs. aliphatics) interface curvature with growing chain length *n*. Due to the metastability only in one case (*n*=18) the hexagonal lattice could be confirmed by XRD and the lattice parameter was found to be $a_{\text{hex}} = 5.07$ nm.^[58] About 5 molecules are arranged side by side in the rafts forming the columnar aggregates. In the Cub_{bi} and Tet_{bi} phases this number is a bit smaller, between 3.2–3.7 molecules (Table 2). We attribute this, at least in part, to the uniformly helical organization of the π -conjugated rods in the network phases, allowing a denser core packing, while the alkyl chain packing is not changed at the Col_{hex}-Cub_{bi} transition. This provides an increased aliphatic-aromatic intermaterials interface curvature leading to the reduction of the diameter of the network cores. Remarkably, for compound A10/14, being at the borderline to the short-chain compounds, the metastable Col_{hex} phase is replaced by Iso₁.^[*]

Polyamorphism in the liquid state. – In the case of the long chain compounds A10/16 to A10/20 there is an extremely broad (30–40 K) and almost symmetric feature in the isotropic liquid range with a maximum around 170°C on heating and around 165°C on cooling, associated with an enthalpy change $\Delta H = 2.5$ –4.0 kJ mol⁻¹ (Table 1 and Figure 3d). The sample remains optically isotropic and fluid in this temperature range and this transition is not associated with conglomerate formation, and therefore this achiral isotropic mesophase range between the Cub_{bi} phase and the maximum of the broad DSC feature is named Iso₁.^[67,68] The reversible and continuous transition between Iso and Iso₁ takes place about 10–20 K above the next phase transition to a (Cub_{bi}/Col_{hex}) LC phase. It is attributed to the continuous transition between the ordinary isotropic liquid phase (Iso) and a percolated Iso₁ phase by the continuous growth of cybotactic clusters of the networks (Figure 6).^[51,68] Upon further cooling this broad feature is followed by a sharp peak at 147–152°C, leading to Col_{hex} followed by the transition to the Cub_{bi}/Ia $\bar{3}d$ phase at around 144°C (Table 1). The total enthalpy of these two transitions is about 2 kJ mol⁻¹ which is a bit smaller than the broad feature in the isotropic range, indicating that major molecular aggregation takes already place in the range of the Iso-Iso₁ transition. Figure 9c shows the dependence of the *d*-spacing and line

width at half maximum (FWHM) of the diffuse SAXS of **A10/14** on continuous heating in the isotropic liquid range. A continuous decrease of the coherence length across the Iso₁–Iso transition is observed in the investigated temperature range of the liquid state. This supports the proposed disruption of the networks at the Cub_{bi}–Iso₁ transition and the almost continuous reduction of the correlation length of network order with further rising temperature (Figure 6).

For compound **A10/12**, representing a short chain compound located at the borderline to the long chain compounds, there are two DSC features in the isotropic liquid range on cooling (Figure 3c), an almost symmetric and very broad one at higher temperature between 155–185 °C and the typical bump with tailing occurring at 162 °C. The latter is again associated with the onset of chirality synchronization by conglomerate formation, whereas no change can be observed in the temperature range of the broad feature. This indicates a liquid state triamorphism due to the continuous emergence and growth of a local network structure in the Iso₁ range, which reaches the critical connectivity for chirality synchronization at the transition to Iso₁^[*] and on further cooling fuses to a long range cubic *I23* network at the next phase transition at 156 °C (Figure 6). In this case a significant molecular aggregation and network formation takes place before chirality synchronization sets in. This kind of triamorphism was previously observed for benzil derived polycatenars.^[51]

For compound **A10/14**, representing a long chain compound at the border line to the short chain compounds the same liquid state triamorphism Iso–Iso₁–Iso₁^[*] is observed, though in this case the achiral Cub_{bi}/*Ia3d* phase is formed instead of the chiral *I23*^[*] phase on further cooling (Table 1, Figure 3). This means that chirality synchronization in the liquid state is supported by decreasing chain length and lowering temperature and that upon chain length reduction the internetwork correlation in the adjacent LC phase changes from enantiophilic for $n = 14$ to enantiophobic for $n = 12$.

Overall, there are two groups of compounds. The short chain compounds with $n = 5–12$ show ambidextrous mirror symmetry breaking in the Cub_{bi}/*I23*^[*] as well as in the Iso₁^[*] phases, whereas for the long chain compounds with $n = 14–20$ the mirror symmetry broken Cub_{bi}/*I23*^[*] and Iso₁^[*] phases are replaced by mesoscale conglomerates (Tet_{bi}/*I23*), and achiral cubic (*Ia3d*), columnar (Col_{hex}) and isotropic liquid (Iso₁) mesophases. Compounds at the transition between these two groups ($n = 12, 14$) show liquid state polyamorphism with a chiral liquid mesophase at low (Iso₁^[*]) and an achiral liquid mesophase (Iso₁) at higher temperature. This indicates that macroscopic mirror symmetry breaking is gradually lost with growing alkyl chain length n with the major change taking place from $n = 12 \rightarrow 14$.

Discussion

LC phase transitions in relation to chirality synchronization

As noted in the Introduction, the Cub_{bi} phases of polycatenar compounds involve a helical organization of the rod-like molecules along the individual networks and the network junctions ensure a uniform helicity along the networks.^[10,17,18,20,37] We hypothesize that the capability of a denser chirality synchronized helical organization of the molecules in the networks of the Cub_{bi} phases is a main reason for the wide ranges of Cub_{bi} phases observed for polycatenar and related rod-like molecules,^[32] while for other classes of compounds, which do not evolve a helical organization,^[36] the Cub_{bi} phases are rare and restricted to narrow chain volume and temperature ranges.^[30–35,69] It appears that this stabilization of the networks by chirality synchronization can even be retained after loss of the long-range cubic lattice in the adjacent mirror symmetry broken isotropic liquid mesophases (Iso₁^[*]), as observed for the short chain compounds **A10/7–A10/12**.

Both, the kind of network structure (topology, number of interwoven networks, valency and geometry of the junctions), as well as the mode of interhelix interactions between adjacent network, being either enantiophobic or enantiophilic, decide if the overall structure becomes a chiral conglomerate or an achiral *meso*-structure.^[58] The Cub_{bi}/*Ia3d* phase is such a *meso*-structure formed by two enantiomorphic networks with opposite helicity, as proven in previous RSoXS investigations of the *Ia3d* phase of compound **A10/18**.^[36] This *meso*-structure is stable as long as the interactions between the two helical networks are more or less enantiophilic, too, i.e. if heterochiral self-assembly between the networks is favored. As the networks are stretched along the *c* direction at the continuous transition to the Tet_{bi} phase the interhelical interaction appears to change from enantiophilic to enantiophobic, i.e. the homochiral self-assembly of adjacent networks becomes favored. This requires that either the network structure changes, or alternatively, uniform helicity is removed in at least one of the networks. It is proposed that the first case leads to the Cub_{bi} phase with chiral *I23* space group, whereas the second case causes a transition to the Tet_{bi} phase. As previously shown for **A10/18**, the Tet_{bi} phase can be considered as an intermediate phase at the transition between the chiral *I23* phase and the achiral *Ia3d* phase.^[58] At the transition to this mirror symmetry broken Tet_{bi} phase the achiral *meso*-structure of the *Ia3d* phase is broken by retaining uniform helicity only along one network, while losing it along the other one. One network is racemized in the *P4*₁*2*₁*2* phase and the other one in the enantiomorphic *P4*₃*2*₁*2* phase. This leads to a pair of chiral space groups *P4*₁*2*₁*2* and *P4*₃*2*₁*2* forming a mesoscale conglomerate, thus providing a new way of mirror symmetry breaking in soft matter by partial *meso*-structure racemization at the transition from enantiophilic to enantiophobic interhelical self-assembly between networks.^[58]

For the compounds **A10/14–A10/18** reported here, there is a competition between the Tet_{bi} and the Cub_{bi}/*I23* phases, the former representing the thermodynamically more stable structure. The notable feature of the *I23* phase of all long chain

compounds is the absence of visible conglomerate formation. This could be explained by relatively weak enantiophobic interhelix interactions, tolerating relatively large contact areas between small domains with opposite chirality (racemic interfaces). Therefore, the chiral domains of the conglomerate retain a small size and cannot be detected by optical microscopy. Overall there appears to be a decreasing strength of the enantiophobic character of the interhelical network interaction and a transition to an enantiophilic interaggregate chirality synchronization with rising chain length n . This leads to a LC phase sequence $\text{Cub}_{\text{bi}}//I23^{[*]}-\text{Cub}_{\text{bi}}/I23-\text{Tet}_{\text{bi}}/P4_12_2/P4_32_12-\text{Cub}_{\text{bi}}/Ia\bar{3}d$ with growing chain length, i.e. it appears that the changing mode of chirophilic self-assembly modulates the phase structure.

Liquid state polyamorphism and mirror symmetry breaking

In line with this change of interaggregate chirality synchronization the polyamorphism in the liquid phase changes, too. While for compounds **A10/5–A10/10** a mirror symmetry broken $\text{Iso}_1^{[*]}$ -phase (presumably with local $I23$ structure) is observed, it is replaced for the long chain compounds **A10/16–A10/20** by an achiral Iso_1 phase. Compounds **A10/12** and **A10/14**, located at the transition between the short and long chain compounds show both, the chiral $\text{Iso}_1^{[*]}$ -phase as well as the achiral Iso_1 phase in the sequence $\text{Iso}-\text{Iso}_1-\text{Iso}_1^{[*]}-\text{Cub}_{\text{bi}}$ on cooling, while the Cub_{bi} type switches from the chiral $I23^{[*]}$ to the achiral $Ia\bar{3}d$ -type at the transition from **A10/12** to **A10/14** (Figure 2).

For the compounds with short chains ($n=5-10$) the absence of any $\text{Iso}-\text{Iso}_1$ transition in the liquid range indicates the absence of notable network formation in the liquid state. This is attributed to the relatively weak segregation between rigid aromatic units and the relatively short flexible alkyl chains. Therefore, chirality synchronization is required for the onset of network formation in the liquid state of the short chain compounds. In a feed-back the evolving networks support macroscopic chirality synchronization. Thus, an $\text{Iso}-\text{Iso}_1^{[*]}$ transition with ambidextrous mirror symmetry breaking is observed, though the driving force of aggregate formation by the self-assembly due to the aromatic-aliphatic segregation is still weak in the liquid state.

In contrast, for the compounds with long chains ($n=16-20$) aromatic-aliphatic segregation becomes stronger, allowing self-assembly by network formation already in the liquid state even in the absence of chirality synchronization. However, on the other hand, there appears to be a weaker driving force for chirality synchronization for these compounds with long chains, leading to the $\text{Iso}-\text{Iso}_1$ transition without mirror symmetry breaking. Only at the transition between these two different modes of liquid state diamorphism, when segregation and chirality synchronization forces are both sufficiently strong, the $\text{Iso}-\text{Iso}_1-\text{Iso}_1^{[*]}$ triamorphism is observed ($n=12, 14$).

Considering the network formation as a dynamic mode of supramolecular polymerization the growth is considered as isodesmic around the $\text{Iso}-\text{Iso}_1$ transition of the long chain compounds and becomes cooperative for the $\text{Iso}-\text{Iso}_1^{[*]}$ tran-

sition of the short chain compounds.^[70] It is noted that supramolecular polymerization is in this case only driven by the nano-scale segregation of the polyaromatic units from the aliphatic molecular segments^[71] and does not involve any specific strong interaction like H-bonding. Therefore, it is sensitive to slight molecular structural modifications like chain length variation.

For the $\text{Iso}_1^{[*]}$ phase occurring besides the $\text{Cub}_{\text{bi}}//I23^{[*]}$ phase a $I23$ -like local triple network structure can be assumed as the most likely structure,^[10] whereas the local structure in the achiral Iso_1 phase is less obvious. It could either be a local helical network with $Ia\bar{3}d$ -like *meso*-structure, as previously proposed for benzil based molecules.^[51] Alternatively, a random network structure without or with only short-range chirality synchronization along the networks can be envisaged. The latter is supported by the very distinct shapes of the $\text{Iso}-\text{Iso}_1$ and $\text{Iso}-\text{Iso}_1^{[*]}$ transitions in the DSC traces, associated with distinct growth mechanisms. The cooperative nature of the $\text{Iso}-\text{Iso}_1^{[*]}$ transitions (distinct DSC peak) suggests that chirality synchronization might be responsible for the cooperativity. A cooperative growth would also be expected if the $Ia\bar{3}d$ -like phase structure would be formed, which is also chirality synchronized, though with opposite sign in the two networks. The isodesmic growth in the case of the achiral Iso_1 phase (broad feature in DSC) is a hint that chirality synchronization is obviously not involved in this transition and therefore a randomized, only short-range helical network structure is proposed for this achiral Iso_1 phase. This is additionally supported by the observation that for all long chain compounds **A10/16–A10/20** an achiral Col_{hex} phase is formed below Iso_1 before the transition to the chirality synchronized $\text{Cub}_{\text{bi}}/Ia\bar{3}d$ phase takes place. For compounds **A10/12** and **A10/14** at the cross-over between short- and long chain compounds the non-helical Iso_1 phase is formed first and chirality synchronization leads to the $I23^{[*]}$ -like local structure at the transition to the $\text{Iso}_1^{[*]}$ range. For compound **A10/12** enantiophobic network coupling is retained at the transition to the chiral $\text{Cub}_{\text{bi}}//I23^{[*]}$ phase, whereas for **A10/14** the transition to the long-range cubic lattice is associated with development of enantiophilic network correlation in the achiral $\text{Cub}_{\text{bi}}/Ia\bar{3}d$ -phase.

Effects of chain length

Though the transition between the $Ia\bar{3}d$ and $I23^{[*]}$ type Cub_{bi} phases with a Tet_{bi} phase as intermediate structure at this transition can be understood by a change of the mode of internetwork chirality synchronization from enantiophilic to enantiophobic, there is still the question how this is related to the molecular structure. The effects of chain elongation can be divided into the *general effects* on mesophase-type and -stability, and the *specific chirality related effects*.

Among the *general effects*, a growing chain length n provides a stronger segregation of the flexible chains from the rod-like units which then supports the self-assembly in the liquid and LC phases. It leads to long-range network formation in the LC phases, and dynamic mesoscale networks in the liquid

state if $n \geq 12$ (Iso–Iso₁ transition). In addition, the chain volume affects the curvature of the intermaterials dividing interfaces and leads to the metastable Col_{hex} phase for long chain compounds with $n = 16$ –20. However, due to the chain disorder around the columns and networks there is no significant odd-even effect for any of the phase transitions (see Figure 2).

The *specific effects* induce helicity and influence the mode and strength of interhelical network coupling. The imbalance between the cross-sectional areas of cores and chains in polycatenar mesogens leads to the helical twist Φ between the rafts of molecules along the networks. Growing chain volume increases Φ and reduces the helical pitch length. Thus, alkyl chain elongation supports the chirality synchronization within the individual networks. However, it is also known that a change of the helical twist can modify the mode of interhelical coupling (enantiophilic vs. enantiophobic) though the precise relations are still largely unknown.^[72–74] The helical pitch length also affects the distances between the network junctions, because the twist between them is a fixed value. If this distance is in conflict with the distances required by amphiphilic self-assembly (e.g. the 70.5° twist between the trigonal junctions in the $la\bar{3}d$ phase), then the phase structure is changed and the spatial orientation between the helical network segments also changes. This leads to a modified helix orientation which can also affect the preferred mode of coupling between the networks. The interplay between both effects gives rise to the complex phase sequences with a transition between enantiophilic and enantiophobic internetwork correlation (Cub_{bi}/ $la\bar{3}d$ -Tet_{bi}–(Cub_{bi}/ $I23$)–Cub_{bi}/ $I23^{[*]}$). There is also an effect of chain length on the strength of chirality synchronization between the networks, because growing chain length decreases the interaggregate interactions (due to growing distances and chain disorder), it reduces the strength of coupling between the networks. As a result, chiral Iso₁^[*] and Cub_{bi}/ $I23^{[*]}$ phases of the short chain compounds are replaced by the achiral Iso₁ phase and the mesoscale conglomerate type Cub_{bi}/ $I23$ phase upon chain elongation.

The sequence $la\bar{3}d_{(L)} \rightarrow I23^{[*]} \rightarrow la\bar{3}d_{(S)}$ was previously found for polycatenar^[32,38,39,50,51] and other rod-like molecules and supramolecules, like bis(4-alkoxybenzoyl)hydrazines (BABH-*n*)^[65,75] and 4'-alkoxy-3'-nitrophenyl-4-carboxylic acid dimers (ANBC-*n*).^[64,76] Also for these compounds birefringent 3D phases as well as Col_{hex} and Iso₁ phases^[32,68] were reported to accompany their cubic phases, especially around the $I23^{[*]}$ – $la\bar{3}d$ transitions.^[22,32,41] The present work provides a preliminary understanding of these phases and their transitions on the basis of the helical self-assembly of the rod-like cores and the effect of the alkyl chains on molecular aggregation, chirophilicity and strength of interhelical coupling.

Summary and Conclusions

In summary, we reported the soft self-assembly of a series of azobenzene-based polycatenars terminated with a 3,4,5-tridecyloxybenzoate moiety at one end and a single alkoxy chain with varying chain length $n = 5$ –20 at the opposite end. For short

and medium chain homologues an ambidextrous chiral Cub_{bi} phase with $I23$ lattice (Cub_{bi}/ $I23^{[*]}$) is observed as stable structure. Some Cub_{bi} phases do not crystallize once formed, making them candidates for technological applications of the chirality synchronized network structures after asymmetry amplification and formation of uniform chirality. For compounds with a longer chain the achiral Cub_{bi} phase with $la\bar{3}d$ lattice (Cub_{bi}/ $la\bar{3}d$) and a tetragonal phase with $P4_12_1/P4_32_2$ lattice were observed as stable LC phases. Overall there appears to be a transition from enantiophobic self-assembly in the chiral $I23^{[*]}$ phase of the short chain compounds to enantiophilic internetwork interactions in the achiral $la\bar{3}d$ phase of the long chain compounds. An apparently achiral $I23$ phase and a tetragonal phase, both representing mesoscale conglomerates, appear as intermediate states at this transition. All compounds show an additional polyamorphism in the isotropic liquid state involving a mirror symmetry broken Iso₁^[*] phase for the short chain compound and an achiral Iso₁ phase for the long chain compounds, both occurring below the ordinary Iso phase. It is concluded that there is a growing general driving force for self-assembly with growing chain length. On the other hand, the strength of interhelical chirality synchronization decreases and the mode of chirophilic internetwork interactions changes from being enantiophobic to enantiophilic by growing alkyl chain length. Thus, in the reported case short chains are favourable for mirror symmetry breaking.

Overall, this work contributes to the understanding of supramolecular polymerization of achiral molecules with properly functionalized π -conjugated units into dynamic helical networks, thus leading to the spontaneous emergence of homochirality in LC network phases and isotropic melts of achiral molecules.^[10,18–20] It is noted that recently a similar mirror symmetry breaking was also observed during solution polymerizations of achiral monomers to covalent helical polymers,^[77] demonstrating the generality of this concept. Owing to the azobenzene units incorporated in the molecular structures photo switching upon light irradiation (see Figure S16) provides additional possibility for these materials to be used in chiroptical and other technological applications.^[1,2]

Experimental Section

Synthesis: The appropriate 4-(4-alkoxyphenyldiazenyl)benzoic acid $1/n$ (1.0 mmol) was converted to the corresponding acid chloride by refluxing under stirring for one hour with excess SOCl₂ (10 mL) and few drops of DMF as a catalyst. The excess SOCl₂ was removed under reduced pressure and 4'-hydroxybiphenyl-4-yl 3,4,5-tridecyloxybenzoate (**2**) (1.0 mmol) dissolved in 25 mL of dry CH₂Cl₂ was added together with Et₃N (1.2 mmol) and a catalytic amount of pyridine. The reaction mixture was refluxed for 6 h. At the end of the reaction as confirmed from the TLC, the mixture was cooled, poured into ice-water (100 mL) and the crude product was extracted with CH₂Cl₂ (3 × 50 mL). The organic layer was washed twice with water and dried over anhydrous MgSO₄ and the solvent was removed under reduced pressure. The resulting orange solid material was purified by column chromatography over silica gel using CH₂Cl₂ as eluent, followed by recrystallization from EtOH/CHCl₃ mixture (3/1, v/v) to give the final compounds as orange crystals (yields: 55–68% purified compounds). The analytical data of

A10/5 are given as representative example; those of all other homologous compounds **A10/n** with $n=6-16$ and 20 are collated in the Supporting Information; compound **A10/18** was reported previously.^[36]

A10/5: ¹H NMR (500 MHz, CDCl₃) δ 8.37 (d, $J=7.9$ Hz, 2H, Ar–H), 8.05–7.90 (m, 4H, Ar–H), 7.77–7.59 (m, 4H, Ar–H), 7.44 (s, 2H, Ar–H), 7.38–7.26 (m, 4H, Ar–H, overlapped with CDCl₃), 7.04 (d, $J=8.3$ Hz, 2H, Ar–H), 4.15–3.99 (m, 8H, Ar–OCH₂CH₂), 1.97–1.68 (m, 8H, Ar–OCH₂CH₂), 1.67–1.17 (m, 46H, 23 × CH₂), 0.97 (t, $J=7.2$ Hz, 3H, CH₃), 0.90 (t, $J=6.9, 3.3$ Hz, 9H, 3 × CH₃). ¹³C NMR (126 MHz, CDCl₃) δ 165.04, 164.75 (C=O), 162.50, 155.87, 152.99, 150.58, 150.45, 146.88, 143.13, 138.30, 138.11 (C_{ar}–O, C_{ar}–N), 131.25, 130.38 (C_{ar}–H), 128.25 (C_{ar}–quart), 128.21, 125.34 (C_{ar}–H), 123.84 (C_{ar}–quart), 122.56, 122.13, 122.04, 114.86, 108.66 (C_{ar}–H), 73.60, 69.31, 68.47 (CH₂O), 31.94, 31.91, 30.35, 29.73, 29.67, 29.63, 29.60, 29.58, 29.57, 29.39, 29.34, 29.32, 28.86, 28.16, 26.09, 26.06, 22.70, 22.68, 22.44 (CH₂), 14.10, 14.00 (CH₃). Elemental analysis, calc. for C₆₇H₉₂N₂O₈: C 76.39%, H 8.80%, N 2.66%, found: C 76.32%, H 8.75%, N 2.59%.

Investigations: POM was conducted with an Optiphot 2 Nikon microscope on a Mettler FP82HT heating stage between non-treated microscopy glass plates with a distance of 10–20 μm. Larger distances were achieved by using a wedge-sell configuration. DSC scans were performed with a DSC-7 and DSC-8000 from Perkin Elmer, with heating and cooling rates of 10 Kmin⁻¹ in aluminium pans (30 μL). In-house XRD was carried out in glass capillaries (1 mm cross section, Hilgenberg) or with open droplets on a glass surface using CuKα radiation ($\lambda=0.154$ nm) and a Vantec 500 area detector. The detector sample distances were 26.80 cm for SAXS and 9.00 cm for WAXS. The samples were held on a self-made temperature-controlled heating stage. High-resolution SAXS patterns were recorded at beamline BL16B1 of Shanghai Synchrotron Radiation Facility (SSRF) with a MarCCD 165 detector. Powder samples were held in capillaries and temperature controlled with a Linkam hot stage. For each temperature, the samples were irradiated 10–120 s to acquire data with enough resolution and signal intensity for electron density map reconstruction.

Acknowledgements

M. Alaasar acknowledges the German Research Foundation (DFG) for the financial support (AL2378/1-1, 424355983 and 43494874 – GRK 2670) and F. Liu acknowledges financial supporting from National Natural Science Foundation of China (21761132033). The authors are grateful to Beamline BL16B1 at SSRF (Shanghai Synchrotron Radiation Facility, China) for providing the beamtime. Open Access funding enabled and organized by Projekt DEAL.

Conflict of Interest

The authors declare no conflict of interest.

Data Availability Statement

The data that support the findings of this study are available in the supplementary material of this article.

Keywords: alkyl chain engineering · azobenzene · chirality · liquid crystals · mirror symmetry breaking

- [1] a) H. K. Bisoyi, Q. Li, *Chem. Rev.* **2022**, *122*, 4887; b) Z. J. Zheng, Y. Q. Lu, Q. Li, *Adv. Mater.* **2020**, *32*, 1905318.
- [2] a) M.-M. Zhang, K. Li, S.-Q. Zang, *Adv. Opt. Mater.* **2020**, *8*, 1902152; b) Y. Zhang, S. Yu, B. Han, Y. Zhou, X. Zhang, X. Gao, Z. Tang, *Matter* **2022**, *5*, 837.
- [3] a) J. L. Pasteur, *Ann. Chim. Phys.* **1848**, *24*, 442; b) E. Yashima, N. Ousaka, D. Taura, K. Shimomura, T. Ikai, K. Maeda, *Chem. Rev.* **2016**, *116*, 13752; c) Y. Wang, J. Xu, Y. Wang, H. Chen, *Chem. Soc. Rev.* **2013**, *42*, 2930; d) T. Matsuura, H. Koshima, *J. Photochem. Photobiol. C* **2005**, *6*, 7; e) D. B. Amabilino, R. M. Kellogg, *Isr. J. Chem.* **2011**, *51*, 1034; f) L. C. Sögütoglu, R. R. Steendam, H. Meeks, E. Vlieg, F. P. Rutjes, *Chem. Soc. Rev.* **2015**, *44*, 6723.
- [4] a) T. Buhse, J. M. Cruz, M. E. Noble-Teran, D. Hochberg, J. M. Ribó, J. Crusats, J. C. Micheau, *Chem. Rev.* **2021**, *121*, 2147; b) B. Chang, X. Li, T. Sun, *Eur. Polym. J.* **2019**, *118*, 365.
- [5] P. J. M. Stals, P. A. Korevaar, M. A. J. Gillissen, T. F. A. de Greef, C. F. C. Fittie, R. P. Sijbesma, A. R. A. Palmans, E. W. Meijer, *Angew. Chem. Int. Ed.* **2012**, *51*, 11297.
- [6] a) M. Liu, L. Zhang, T. Wang, *Chem. Rev.* **2015**, *115*, 7304; b) Y. Sang, M. Liu, *Chem. Sci.* **2022**, *13*, 633.
- [7] C. Tschierske, *Angew. Chem. Int. Ed.* **2013**, *52*, 8828.
- [8] *Handbook of Liquid Crystals*, 2nd ed. (Eds.: J. W. Goodby, P. J. Collings, T. Kato, C. Tschierske, H. Gleeson, P. Raynes) Wiley-VCH, Weinheim, Germany, **2014**.
- [9] a) T. Kato, J. Uchida, T. Ichikawa, T. Sakamoto, *Angew. Chem. Int. Ed.* **2018**, *57*, 4355; b) D. L. Gin, X. Lu, P. R. Nemade, C. S. Pecinovsky, Y. Xu, M. Zhou, *Adv. Funct. Mater.* **2006**, *16*, 865; c) J. Voskuhl, M. Giese, *Aggregate* **2022**, *3*, e124; d) J. Uchida, B. Soberats, M. Gupta, T. Kato, *Adv. Mater.* **2022**, 2109063; e) Y.-K. Kim, J. H. Noh, K. Nayani, N. L. Abbott, *Soft Matter* **2019**, *15*, 6913.
- [10] a) C. Tschierske, G. Ungar, *ChemPhysChem* **2016**, *17*, 9; b) C. Tschierske, *Liq. Cryst.* **2018**, *45*, 2221.
- [11] a) H. Takezoe, *Top. Curr. Chem.* **2012**, *318*, 303; b) K. V. Le, H. Takezoe, F. Araoka, *Adv. Mater.* **2017**, *29*, 1602737.
- [12] a) Y. Takahashi, G. J. Shin, J. C. Jung, S.-W. Choi, K. Ishikawa, J. Watanabe, H. Takezoe, P. Toledano, *J. Mater. Chem.* **2005**, *15*, 4020; b) J. Thisayukta, Y. Nakayama, S. Kawachi, H. Takezoe, J. Watanabe, *J. Am. Chem. Soc.* **2000**, *122*, 7441.
- [13] a) G. Dantlgraber, A. Eremin, S. Diele, A. Hauser, H. Kresse, G. Pelzl, C. Tschierske, *Angew. Chem. Int. Ed.* **2002**, *41*, 2408; b) L. E. Hough, M. Spannuth, M. Nakata, D. A. Coleman, C. D. Jones, G. Dantlgraber, C. Tschierske, J. Watanabe, E. Körblova, D. M. Walba, J. E. MacLennan, M. A. Glaser, N. A. Clark, *Science* **2009**, *325*, 452.
- [14] a) S. P. Sreenilayam, Y. P. Panarin, J. K. Vij, V. P. Panov, A. Lehmann, M. Poppe, M. Prehm, C. Tschierske, *Nat. Commun.* **2016**, *7*, 11369; b) A. Lehmann, M. Alaasar, M. Poppe, S. Poppe, M. Prehm, M. Nagaraj, S. P. Sreenilayam, Y. P. Panarin, J. K. Vij, C. Tschierske, *Chem. Eur. J.* **2020**, *26*, 4714.
- [15] R. Oikawa, H. Sasaki, Y. Takanishi, M. Sagisaka, J. Yamamoto, A. Yoshizawa, *Soft Matter* **2019**, *15*, 3179.
- [16] a) V. Borshch, Y.-K. Kim, J. Xiang, M. Gao, A. Jákli, V. P. Panov, J. K. Vij, C. T. Imrie, M. G. Tamba, G. H. Mehl, O. D. Lavrentovich, *Nat. Commun.* **2013**, *4*, 2635; b) M. R. Tuchband, D. A. Paterson, M. Salamonczyk, V. A. Normand, A. N. Scarbrough, E. Forsyth, E. Garcia, C. Wang, J. M. D. Storey, D. M. Walba, S. Sprunt, A. Jákli, C. Zhu, C. T. Imrie, N. A. Clark, *Proc. Natl. Acad. Sci. USA* **2019**, *116*, 10698; c) R. J. Mandle, J. W. Goodby, *Chem. Eur. J.* **2019**, *25*, 14454; d) Y. Cao, J. Feng, A. Nallapaneni, Y. Arakawa, K. Zhao, H. Zhang, G. H. Mehl, C. Zhu, F. Liu, *J. Mater. Chem. C* **2021**, *9*, 10020; e) M. M. Majewska, E. Forsyth, D. Pocięcha, C. Wang, J. M. D. Storey, C. T. Imrie, E. Gorecka, *Chem. Commun.* **2022**, *58*, 5285.
- [17] C. Dressel, F. Liu, M. Prehm, X. Zeng, G. Ungar, C. Tschierske, *Angew. Chem. Int. Ed.* **2014**, *53*, 13115.
- [18] C. Dressel, T. Reppe, M. Prehm, M. Brautzsch, C. Tschierske, *Nat. Chem.* **2014**, *6*, 971.
- [19] C. Dressel, W. Weissflog, C. Tschierske, *Chem. Commun.* **2015**, *51*, 15850.
- [20] C. Tschierske, C. Dressel, *Symmetry* **2020**, *12*, 1098.
- [21] a) A. Guijarro, M. Yus, *The origin of chirality in the molecules of life*, RSC Publishing, Cambridge, UK, **2009**; b) Q. Sallembien, L. Bouteiller, J. Crassous, M. Raynal, *Chem. Soc. Rev.* **2022**, *51*, 3436.
- [22] a) H. T. Nguyen, C. Destrade, J. Malthete, *Adv. Mater.* **1997**, *9*, 375; b) D. W. Bruce, *Acc. Chem. Res.* **2000**, *33*, 831; c) W. Weissflog, in

- Handbook of Liquid Crystals*, 2nd Ed., (Eds. J. W. Goodby, J. P. Collings, T. Kato, C. Tschierske, H. F. Gleeson, P. Raynes), Vol. 5, Wiley-VCH, Weinheim, Germany, 2014, pp. 89–174.
- [23] A. Zehnacker, M. A. Suhm, *Angew. Chem. Int. Ed.* **2008**, *47*, 6970.
- [24] R. P. Lemieux, *Chem. Soc. Rev.* **2007**, *36*, 2033.
- [25] M. Lehmann, M. Hügel, *Angew. Chem. Int. Ed.* **2015**, *54*, 4110.
- [26] H. Nagayama, S. K. Varshney, M. Goto, F. Araoka, K. Ishikawa, V. Prasad, H. Takezoe, *Angew. Chem. Int. Ed.* **2010**, *49*, 445.
- [27] a) Y.-X. Li, H.-F. Gao, R.-B. Zhang, K. Gabana, Q. Chang, G. A. Gehring, X.-H. Cheng, X.-B. Zeng, G. Ungar, *Nat. Commun.* **2022**, *13*, 384; b) P. Rybak, A. Krowczynski, J. Szydłowska, D. Pocięcha, E. Gorecka, *Soft Matter* **2006**, *18*.
- [28] a) V. Percec, M. Peterca, T. Tadjiev, X. Zeng, G. Ungar, P. Leowanawat, E. Aqad, M. R. Imam, B. M. Rosen, U. Akbey, R. Graf, S. Sekharan, D. Sebastiani, H. W. Spiess, P. A. Heiney, S. D. Hudson, *J. Am. Chem. Soc.* **2011**, *133*, 12197; b) C. Roche, H. J. Sun, M. E. Prendergast, P. Leowanawat, B. E. Partridge, P. A. Heiney, F. Araoka, R. Graf, H. W. Spiess, X. Zeng, G. Ungar, V. Percec, *J. Am. Chem. Soc.* **2014**, *136*, 7169; c) V. Percec, Q. Xiao, *Isr. J. Chem.* **2021**, *61*, 530.
- [29] A mesophase is considered as LC as long as there is only diffuse scattering in the WAXS range.^[31]
- [30] J. M. Seddon, R. H. Templer, *Polymorphism in Lipid-Water Systems. In Handbook of Biological Physics* (Eds.: R. Lipowsky, E. Sackman), Elsevier: Amsterdam, The Netherlands, 1995, Volume 1, pp. 97–160.
- [31] G. Ungar, F. Liu, X. Zeng, *Cubic and 3D Thermotropic Liquid Crystal Phases and Quasicrystals. In Handbook of Liquid Crystals 2nd Ed.* (Eds.: J. W. Goodby, P. J. Collings, T. Kato, C. Tschierske, H. Gleeson, P. Raynes), Wiley-VCH, Weinheim, Germany, 2014; Volume 5, pp. 363–436.
- [32] S. Kutsumizu, *Isr. J. Chem.* **2012**, *52*, 844.
- [33] A. J. Meuler, M. A. Hillmyer, F. S. Bates, *Macromolecules* **2009**, *42*, 7221.
- [34] S. Hyde, S. Andersson, K. Larsson, Z. Blum, T. Landh, S. Lidin, B. W. Ninham, *The Language of Shape, The Role of Curvature in Condensed Matter: Physics, Chemistry and Biology*; Elsevier, Amsterdam, The Netherlands, 1997.
- [35] L. Han, S. Che, *Adv. Mater.* **2018**, *30*, 1705708.
- [36] Y. Cao, M. Alaasar, A. Nallapaneni, M. Salamończyk, P. Marinko, E. Gorecka, C. Tschierske, F. Liu, N. Vaupotič, C. Zhu, *Phys. Rev. Lett.* **2020**, *125*, 027801.
- [37] X. Zeng, G. Ungar, *J. Mater. Chem. C* **2020**, *8*, 5389.
- [38] C. Dressel, T. Reppe, S. Poppe, M. Prehm, H. Lu, X. Zeng, G. Ungar, C. Tschierske, *Adv. Funct. Mater.* **2020**, 2004353.
- [39] M. Alaasar, A. F. Darweesh, X. Cai, F. Liu, C. Tschierske, *Chem. Eur. J.* **2021**, *27*, 14921.
- [40] Before discovery of its intrinsic chirality, the cubic I23 phase (being one of the “smectic D” phases^[75,76]) was considered to have an $Im\bar{3}m$ lattice with an exceptional large lattice parameter.^[41,42] After discovery of chirality^[17] it was first attributed to the chiral space group I432^[53] before the present I23 model was proposed.^[37] Besides the triple network I23 lattice other alternative models are presently under discussion, see refs. [43,44,47,48] In contrast to these other models, the I23 model in ref. [37] is a triple network structure with junctions having all the same valence of three, the same as in the adjacent $la\bar{3}d$ phases with only two networks.
- [41] A. M. Levelut, M. Clerc, *Liq. Cryst.* **1998**, *24*, 105.
- [42] X. B. Zeng, G. Ungar, M. Imperor-Clerc, *Nat. Mater.* **2005**, *4*, 562.
- [43] K. Saito, Y. Yamamura, Y. Miwa, S. Kutsumizu, *Phys. Chem. Chem. Phys.* **2016**, *18*, 3280.
- [44] S. Kutsumizu, S. Miisako, Y. Miwa, M. Kitagawa, Y. Xamamura, K. Saito, *Phys. Chem. Chem. Phys.* **2016**, *18*, 17341.
- [45] N. Vaupotic, M. Salamonczyk, J. Matraszek, M. Vogrin, D. Pocięcha, E. Gorecka, *Phys. Chem. Chem. Phys.* **2020**, *22*, 12814.
- [46] J. M. Wolska, J. Wilk, D. Pocięcha, J. Mieczkowski, E. Gorecka, *Chem. Eur. J.* **2017**, *23*, 6853.
- [47] W. Lewandowski, N. Vaupotič, D. Pocięcha, E. Gorecka, L. M. Liz-Marzán, *Adv. Mater.* **2020**, 1905591.
- [48] T. Grabovac, E. Gorecka, D. Pocięcha, N. Vaupotic, *Crystals* **2021**, *11*, 214.
- [49] T. Kajitani, S. Kohmoto, M. Yamamoto, K. Kishikawa, *Chem. Mater.* **2005**, *17*, 3812.
- [50] T. Reppe, C. Dressel, S. Poppe, C. Tschierske, *Chem. Commun.* **2020**, 56, 711.
- [51] a) T. Reppe, S. Poppe, X. Cai, F. Liu, C. Tschierske, *Chem. Sci.* **2020**, *11*, 5902; b) T. Reppe, S. Poppe, C. Tschierske, *Chem. Eur. J.* **2020**, *26*, 16066.
- [52] Few other molecular structures forming chirality synchronized cubic phases were reported in refs. [19,43–46,49].
- [53] M. Alaasar, S. Poppe, Q. Dong, F. Liu, C. Tschierske, *Chem. Commun.* **2016**, 52, 13869.
- [54] a) O. Kwon, X. Cai, W. Qu, F. Liu, J. Szydłowska, E. Gorecka, M. J. Han, D. K. Yoon, S. Poppe, C. Tschierske, *Adv. Funct. Mater.* **2021**, *31*, 2102271; b) O. Kwon, X. Cai, A. Saeed, F. Liu, S. Poppe, C. Tschierske, *Chem. Commun.* **2021**, 57, 6491.
- [55] a) M. Alaasar, J. C. Schmidt, X. Cai, F. Liu, C. Tschierske, *J. Mol. Liq.* **2021**, *332*, 115870; b) M. Alaasar, S. Poppe, Y. Cao, C. Chen, F. Liu, C. Zhu, C. Tschierske, *J. Mater. Chem. C* **2020**, *8*, 12902; c) M. Alaasar, S. Poppe, Q. Dong, F. Liu, C. Tschierske, *Angew. Chem. Int. Ed.* **2017**, *56*, 10801; d) M. Alaasar, S. Poppe, C. Tschierske, *J. Mol. Liq.* **2019**, *277*, 233; e) M. Alaasar, X. Cai, Y. Cao, F. Liu, *New J. Chem.* **2022**, *46*, 15871.
- [56] M. Alaasar, M. Prehm, Y. Cao, F. Liu, C. Tschierske, *Angew. Chem. Int. Ed.* **2016**, *55*, 320.
- [57] a) H. Chen, R. Zhang, H. Gao, H. Cheng, H. Fang, X. Cheng, *Dyes Pigm.* **2018**, *149*, 512; b) N. G. Nagaveni, M. Gupta, A. Roy, V. Prasad, Veena, *J. Mater. Chem.* **2010**, *20*, 9089.
- [58] Y. Cao, M. Alaasar, L. Zhang, C. Zhu, C. Tschierske, F. Liu, *J. Am. Chem. Soc.* **2022**, *144*, 6936.
- [59] J.-S. Seo, Y.-S. Yoo, M.-G. Choi, *J. Mater. Chem.* **2001**, *11*, 1332.
- [60] a) M. Sano, T. Kunitake, *Langmuir* **1992**, *8*, 320; b) M. Sano, D. Y. Sasaki, M. Isayama, T. Kunitake, *Langmuir* **1992**, *8*, 1893.
- [61] a) C. L. Folcia, I. Alonso, J. Ortega, J. Etxebarria, I. Pintre, M. B. Ros, *Chem. Mater.* **2006**, *18*, 4617; b) F. Vera, R. M. Tejedor, P. Romero, J. Barberrá, M. B. Ros, J. L. Serrano, T. Sierra, *Angew. Chem. Int. Ed.* **2007**, *46*, 1873.
- [62] a) M. Alaasar, M. Prehm, M. Nagaraj, J. K. Vij, C. Tschierske, *Adv. Mater.* **2013**, *25*, 2186; b) M. Alaasar, M. Prehm, K. May, A. Eremin, C. Tschierske, *Adv. Funct. Mater.* **2014**, *24*, 1703.
- [63] L.-L. Lai, F.-Y. Su, Y.-J. Lin, C.-H. Ho, E. Wang, C.-H. Hung, Y.-H. Liu, Y. Wan, *Helv. Chim. Acta.* **2002**, *85*, 1517.
- [64] S. Kutsumizu, K. Morita, T. Ichikawa, S. Yano, S. Nojima, T. Yamaguchi, *Liq. Cryst.* **2002**, *29*, 1447.
- [65] a) S. Kutsumizu, H. Mori, M. Fukatami, S. Naito, K. Sakajiri, K. Saito, *Chem. Mater.* **2008**, *20*, 3675; b) Y. Yamamura, Y. Nakazawa, S. Kutsumizu, K. Saito, *Phys. Chem. Chem. Phys.* **2019**, *21*, 23705.
- [66] That the Φ -ranges overlap a bit can be attributed to the simultaneous elongation of the molecule by alkyl chain expansion which tends to reduce Φ and to the different temperatures of the measurements.
- [67] Iso–Iso₁ transitions were previously reported to occur besides chirality frustrated LC phases of chiral compounds (BP, TGB) and besides cubic LC phases, see.^[32,68]
- [68] J. W. Goodby, D. A. Dunmur, P. J. Collings, *Liq. Cryst.* **1995**, *19*, 703.
- [69] K. Borisch, S. Diele, P. Göring, H. Kresse, C. Tschierske, *J. Mater. Chem.* **1998**, *8*, 529.
- [70] a) T. F. A. De Greef, M. M. J. Smulders, M. Wolffs, A. P. H. J. Schenning, R. P. Sijbesma, E. W. Meijer, *Chem. Rev.* **2009**, *109*, 5687; b) M. Hartlieb, E. D. H. Mansfield, S. Perrier, *Polym. Chem.* **2020**, *11*, 1083; c) T. Aida, E. W. Meijer, *Isr. J. Chem.* **2020**, *60*, 33.
- [71] C. Tschierske, *Isr. J. Chem.* **2012**, *52*, 935.
- [72] a) A. B. Harris, R. D. Kamien, T. C. Lubensky, *Rev. Mod. Phys.* **1999**, *71*, 1745; b) E. Efrati, W. T. M. Irvine, *Phys. Rev. X* **2014**, *4*, 011003; c) G. M. Grason, *Rev. Mod. Phys.* **2015**, *87*, 401.
- [73] a) J. Lin, Z. Guo, J. Plas, D. B. Amabilino, S. De Feyter, A. P. Schenning, *Chem. Commun.* **2013**, 49, 9320; b) F. Xu, I. J. Khan, K. McGuinness, A. S. Parmar, T. Silva, N. S. Murthy, V. Nanda, *J. Am. Chem. Soc.* **2013**, *135*, 18762; c) S. Díaz-Cabrera, Y. Dorca, J. Calbo, J. Aragón, R. Gómez, E. Ortí, L. Sánchez, *Chem. Eur. J.* **2018**, *24*, 2826.
- [74] E. Frezza, A. Ferrarini, H. B. Kolli, A. Giacometti, G. Cinacchi, *Phys. Chem. Chem. Phys.* **2014**, *16*, 16225.
- [75] D. Demus, G. Kunicke, J. Neelsen, H. Sackmann, *Z. Naturforsch. A* **1968**, *23*, 84.
- [76] G. W. Gray, B. Jones, F. Marson, *J. Chem. Soc.* **1957**, 393.
- [77] G. Yin, T. Namikoshi, M. Teraguchi, T. Kaneko, T. Aoki, *Polymer* **2022**, *245*, 124673.

Manuscript received: June 15, 2022

Accepted manuscript online: July 22, 2022

Version of record online: October 5, 2022